Mechanical Conditions At a Crack Tip and their Effect on Initiation and Growth of Environmentally Assisted Cracking.

Ståhle, P.; Nilsson, Fred; Ljungberg, L. G.

Published in:
Corrosion 88

1988

Document Version:
Publisher's PDF, also known as Version of record

PAPER NUMBER

281

Corrosion 88

March 21-25, 1988
Cervantes Convention Center / St. Louis, Missouri

MECHANICAL CONDITIONS AT A CRACK TIP AND THEIR EFFECT ON INITIATION AND GROWTH OF ENVIRONMENTALLY ASSISTED CRACKING

P. Ståhle and F. Nilsson
Uppsala Institute of Technology
Box 534
S-751 21 Uppsala, Sweden

L. G. Ljungberg
ASEA-ATOM
Box 53
S-721 04 Västerås, Sweden

ABSTRACT

Elasto plastic analysis was performed to determine the conditions at the root of a notch in a CERT specimen and the conditions at a crack growing in a CERT specimen. Furthermore, analysis of growth under small scale yielding was performed in order to facilitate analysis of compact tension specimens. By experiments it was shown how the stress strain conditions affect initiation of intergranular cracking from an air generated transgranular precrack in simulated BWR environments with controlled additions of impurities. The experiments were made on annealed and sensitized Type 304 stainless steel.

INTRODUCTION

Intergranular stress corrosion cracking (IGSCC) of sensitized stainless steel is one of the major operational disturbances to boiling water reactors (BWRs). Traditionally, it has been regarded as a corrosion problem, and at first the major approach to its resolution was by go/no go tests like the constant elongation rate tensile (CERT) technique. However, after the fundamentals of the problem got known it was realized that quantitative data on crack propagation rates were also needed,

and quantitative tests under both constant nominal load and fatigue conditions were started. An early observation was that the crack propagation rates could be correlated to a mechanical variable, the stress intensity factor K_I, and that tests can be performed in such a way that these data are possible to obtain. However, there are situations when the straightforward K_I description fails. It has, for example, been observed that when abrupt changes of the K_I value are made, transient effects on the crack growth rates occur. Another case when the K_I description does not work is when extensive plastic deformation takes place, as, for example, during crack growth in CERT testing.

It is the object of the present paper to attempt analyses of these situations in order to increase the understanding of how mechanical conditions affect crack growth rates. In addition a stress-strain analysis of an uncracked but notched CERT specimen is performed with the object to clarify the mechanical state at crack growth initiation.

All tests described in this paper were run using material from the same heat of Type 304 stainless steel, sensitized by heat treatment 680°C for 1 hour, and subsequently at 500°C for 24 hours. In the calculations the material was assumed to be isotropically elasto-plastic with a linear strain hardening derived from tensile testing.

EXPERIMENTAL PROCEDURE AND TYPICAL RESULTS

In the ASEA-ATOM laboratory, and in test loops in various Swedish boiling water reactors (BWRs), experiments were conducted using constant elongation rate tensile (CERT) tests, corrosion fatigue (CF) tests, and constant load (COL) tests.

Constant Elongation Rate

CERT tests give qualitative results. We use round bar specimens with a mid-gage circumferential V-notch as shown by Figure 1. Before start of a test the specimen is prestressed to betweeen 80 to 90 per cent of the yield stress (at the temperature 288°C) as calculated for the cross section at the bottom of the V-notch, with no regard to notch effects from the V-shape. Subsequently the specimen is strained in the test environment at a nominal rate of $5 \cdot 10^{-8}$ s^{-1} as calculated on the 25 mm gage length. After 168 hrs the test is interrupted, the specimens pulled to fracture in air, and the fracture surface inspected for environmentally assisted cracking. The maximum penetration of environmental cracking on the fracture surface is divided by the test time, and the resulting average crack propagation rate for the time of the test is used as a measure of

susceptibility to environmental cracking.

The way of applying the CERT technique in these tests differs from the way it is normally done. Traditionally unnotched specimens are used which are strained in the test environment until fracture[1]. The strain rate applied when testing stainless steel in high temperature water usually is in the range from 10^{-7} to above 10^{-6} s^{-1}.

There were several objectives for applying a different CERT test technique:

* When testing with a notch, cracking will only occur at the notch, while testing with a smooth specimen will generate several cracks along the length of the test specimen. In the former case, the crack penetration may be taken as a relative measure of the susceptibility to cracking. This is not possible in the case of a smooth specimen, as the crack propagation rate for each crack will depend on the number of cracks and their relative sizes.
* The notch will stimulate crack initiation. The purpose of the tests was to identify water chemistries which were innocuous with regard to environmentally assisted cracking. Thus it was found to be a sound philosophy to search for those chemistries which were not able to sustain crack propagation, rather than those in which crack initiation was difficult although propagation could occur.
* According to the authors' experience, crack initiation when testing with the notch occurs at approximately one per cent of bulk deformation in the specimen gage length. In a smooth specimen several per cent of deformation is required for crack initiation[2]. With the present way of testing the total bulk deformation will be three per cent, while when testing in the conventional way the material will receive several tens of per cent of bulk deformation before fracture.

In studies on the effect of water impurities on environmental cracking the stress strain conditions at the notch also seem to affect the outcome of the test. Nitrate in normal BWR water chemistry seems to have a beneficial effect[3]. However, laboratories using conventional CERT testing techniques find the opposite result, references[4, 5, 6]. It is believed that the difference in results reflects that nitrate enhances crack initiation, but after a crack environment has been established nitrate will be reduced to ammonium before reaching the crack tip which will alleviate crack propagation[4]. This view-point is supported by the present results in hydrogen water chemistry, which when clean does not promote cracking, while in nitrate bearing environment one to two austenite grains deep cracks form.

With other water impurities similar discrepancies between CERT tests with notched and unnotched specimens are also seen. Another example is the effect of carbon dioxide in normal BWR water chemistry, which we think enhances initiation but does not affect propagation[7].

Corrosion Fatigue and Constant Load Tests

CF and COL tests are run to produce quantitative data which may be used to estimate crack propagation rates in reactor applications. For both types of tests, one-inch compact tension (CT) specimens according to ASTM E399, Annex A4, are used. In the CF tests, crack propagation is monitored by crack opening displacement (COD) technique, in the COL tests by potential drop technique (PDT).

The COL tests were run at a wide range of loads given by K_I values from 25 MPa $m^{1/2}$ and upwards. In contrast to the CF tests only intergranular cracking occurred. In very clean environment (with 200 ppb O_2) cracking only occurred at very high K_I, above 40 MPa $m^{1/2}$. In unclean environment, cracking occurred in the whole range of loads tested, generally at decreasing rate with decreasing loads. However, there was always an initiation time of a few days to several weeks during which the crack propagation rate gradually increased from zero to a steady state.

FEM ANALYSIS OF AN UNCRACKED CERT SPECIMEN

In order to obtain a better understanding of the CERT test, the stress and strains were determined by FEM analysis. The first analysis was done on an uncracked specimen and is thus relevant only as long as crack growth initiation has not occurred. For the analysis the program system ABAQUS[8] was used and large deformation behavior was assumed. The finite element mesh is depicted in Figure 1. The material was assumed to be elastic-plastic with linear strain hardening according to the Mises yield criterion and the associated flow rule. From tensile tests at 288^0C the yield stress was found to be σ_Y=160 MPa, and the tangent modulus 0.01 E which equals $1.96 \cdot 10^3$ MPa. Poisson's ratio equals 0.3. These material properties are assumed in all calculations reported below.

The boundary conditions were taken as those used in the experimental procedure, i.e., a momentary deformation to 90 percent of the yield stress σ_Y, and thereafter a constant elongation rate is imposed. In Figure 2 some results for stresses and strains are shown as functions of time. The X:s show the maximum axial stress at the notch surface. This occurs somewhat (0.004 mm) above the symmetry plane. No particular significance should be given to this fact since the maximum is rather flat and the precise location of the stress maximum depends on the FEM discretization. As seen from the figure the stresses are very high, about a factor of 8 larger than the initial yield stress. The hoop stress (open circles) is also shown. It is noted that it is almost as high as the axial stress and thus a nearly cylindrical stress prevails. This is an important difference between the unnotched and the notched CERT specimens and can be of significance for initiation of cracking.

In Figure 2 the maximum axial strain is plotted. There is a tendency for decreasing strain rate with time. The vertical broken line shows the estimated time for crack growth initiation as discussed above. The axial strain at that point of time is about 7 percent.

CRACK GROWTH UNDER TRANSIENT SMALL-SCALE YIELDING CONDITIONS

In the constant load (COL) tests there were various types of observations on crack propagation behavior as a result of load transients which may indicate the stress strain conditions at the crack tip.

A frequent observation, which may be seen in Figures 3 and 4, was that crack propagation rates seemed to decelerate some time after steady state propagation conditions were achieved. It was found that if such a specimen is unloaded once, an immediate increase in crack length was measured. Examples of this may be seen in Figure 3 (at 700 hrs) and in Figure 4 (at 495 hrs and 530 hrs). It was also observed that the temporary increase in measured crack length was dependent on the time (or growth) that had passed since the last such transient. There are two alternative attempts to explain this observation. One possibility is that there are bridges of metal between separate cracks (as may be observed on broken-up cracks) which become broken by the mechanical transient. The other possibility is that electrical connections become separated and oxidized by the transient, in which case the sudden crack increase measured is an artifact of the PDT technique.

Another observation of interest is that a small decrease in K_I will lead to nearly complete crack arrest. Figure 5 is from a laboratory test, where K_I was decreased from 54 to 40 MPa $m^{1/2}$. The crack stopped completely, but after a few hundred hours there was a tendency that the crack started to propagate again. This effect is believed to be due to stress and strain redistribution when changing the loading conditions, and it is one of the main objectives of this article to perform a mechanical analysis of these situations.

An analysis considering the full geometry including the details of the vicinity of the crack tip can, however, not be done in one single computation, not even with very effective computers, at least not at a reasonable computer cost.

Since a detailed analysis is needed to clarify the mechanical behavior of the near tip region a FEM technique which takes advantage of the self similarity of the steady state problem is invoked. Here a code for a moving mesh technique is used to compute the steady state. The entire mesh is moving with the crack tip, and the stress strain distribution is constant when referred to the element mesh. The solution is thus a steady state solution and it can be obtained in one single step.

The full details of the algorithm are described in reference[9] and modifications due to the present problem in reference[10].

A plane body is assumed to have a straight through-crack, which has extended under steady-state plane strain conditions in the crack tip surrounding. The remotely applied load is a uniaxial stress field directed normal to the crack plane The influence of inertia is neglected. A coordinate system is introduced with $x=0$ and $y=0$ at the right crack tip. The crack occupies the region $-2a<x<0$, $y=0$. Due to symmetry of the problem, and by invoking the assumptions of small scale yielding, the only a surrounding of the crack tip at $x=0$, $y=0$, say $-C<x<C$, $0<y<C$, need to be considered.

Polar coordinates (r,θ) are introduced with $r=0$ at the crack tip (see Figure 6). The boundary condition for the case of small scale yielding

$$\sigma_{ij} = \frac{K_I}{\sqrt{2\pi r}} f_{ij}(\theta) \qquad \text{for } r \to \infty \qquad (1)$$

where $f_{ij}(\theta)$ are known functions.
In order to develop an asymptotic approach solution within the limitations of the method applied, loads could not be greater than $K_I = 1.25\sigma_Y C$, since at larger loads small scale yielding could not be maintained.

The shape of the plastic zone extended to about 1/4 of the linear extension of the mesh C. Size and shape are in accordance with the result[9] for a perfectly plastic material (see Figure 7). Very similar shapes and sizes are also reported[9] for materials with about the same hardening rate as the material used in the present study.

The largest extension of the plastic zone in the y-direction is found to be $0.158\,(K_I/\sigma_Y)^2$. The largest extension in the x-direction is $0.119(K_I/\sigma_Y)^2$ and the extension straight ahead of the crack tip is $0.063(K_I/\sigma_Y)^2$. Thus the plastic zone is comparatively thin in the plane $y=0$.

A secondary plastic zone was developed in the wake adjacent to the crack surface. This zone is observed to increase in width and assumes its full width $0.0098(K_I/\sigma_Y)^2$ at a distance about $0.030(K_I/\sigma_Y)^2$ behind the crack tip. The full width is covered by 4 elements.

Obviously an asymptotic solution should be found within the field where the regions of different material behavior divide the near tip field in angular sectors. In the present study three distinctly different kinds of sectors are discovered (see Figure 6), e.g., active plastic (P), linearly elastic wake (W), and secondary plastic (S) sectors. The boundary between the sectors (P) and (W) is found at $\theta_p = 127^0$, and between the the sectors (W) and (S) is found at

$\theta_s = 173^0$. This should be compared with $\theta_p = 123^0$ and $\theta_s = 160^0$ found for the perfectly plastic material[11]. A much larger value for the boundary between (P) and (W) sectors, $\theta_p = 154^0$, is reported[12] for the linearly hardening material. The angle θ is estimated to 179.9^0. The stress distribution corresponds well to the results for the near tip field for a perfectly plastic material[11]. To our surprise the deviation from the result for the near tip field for a linearly hardening material is substantial.

The crack surface displacement v is shown in Figure 8. It has been shown[11] that the asymptotic radial dependence for the displacements for a linearly hardening material can be written r^s, where s is a material property. Thus a solution of the form $v = kr^s$ approximating v in the region $r<0.017(K/\sigma)^2$ - covering 12 nodes - was sought by means of the least squares method. The result suggested that $v \sim r^{0.69}$ which is far from what was found for the asymptotic field for the linearly hardening material[12], namely $v \sim r^{0.9203}$.

The surprising similarities between the present result and asymptotic field for a perfectly plastic material[11] and the significant deviation from the asymptotic field for a linearly hardening material suggested an investigation from a new viewpoint of an example provided by reference[12].

It can be shown for the anti-plane strain (mode III) case that two solutions exist for small values of the ratio $\alpha = E_t/E$, namely $r^{-\sqrt{\alpha}}$ and $r^{\sqrt{\alpha}}$. By choosing a model boundary value problem with reasonable boundary conditions remote from the crack tip, it is shown[12], that a two-term solution approaches the result for a perfectly plastic material as the hardening rate α approaches zero. It is rewarding however, to compare the two-term solution for a finite hardening rate with the dominating term approximation, and secondly with the result for the perfectly plastic material. Thus the displacement rates are chosen for inspection where:

$$\dot{w}_{tt} = \dot{a}\,\frac{\beta^{\tau}Y}{2sG}\,[(r/R)^{-s} - (r/R)^{s}] \qquad (2)$$

is first compared with

$$\dot{w}_{st} = \dot{a}\,\frac{\beta^{\tau}Y}{2sG}\,(r/R)^{-s} \qquad (3)$$

and secondly with

$$\dot{w}_{pp} = \dot{a}\,\frac{\beta^{\tau}Y}{G}\,\ln(R/r) \qquad (4)$$

Here w is the out-of-plane displacement, β is nondimensional and equals 0,3373, dots denote time differentiation, G is the shear modulus, τ_Y is the shear yield stress, R is a length parameter of the order of the linear extension of the plastic zone, and a is the crack length. For s=0.1 the result is that w_{tt} (assumed to be the exact solution) is approximated within 10% by w_{st} for

$$r < 10^{-5} R \tag{5}$$

Thus the approximation w_{st} is applicable only in an extremely small region surrounding the crack tip. Unfortunately the size of this region is certainly much smaller than the size of the fracture process region. Note that a necessary condition when employing the asymptotic field in the analysis is that the field completely embeds the process region.

On the other hand w_{tt} is approximated (within 10%) by the solution for the perfectly plastic material w_{pp} within the range

$$4.3 \cdot 10^{-4} R < r < R \tag{6}$$

which covers the essential part of the plastic zone (see Figure 6). The region $r<4.3 \cdot 10^{-4} R$, where the approximation cannot describe the displacements, is generally insignificant when compared with the extension of the process region.

Returning to the mode I case it is, in view of the present FEM result, assumed that the perfectly plastic solution[11] for mode I is the proper approximation of the mechanical behavior in the near tip region, in analogy with what was found for the mode III case. It is also assumed that the asymptotic solution[12] for the linearly hardening material resides in an extremely close vicinity of the crack tip. The amplitude for the solution[10] is determined by simple curve fitting. Thus

$$v_a = 3.11 \frac{\sigma_Y}{E} r \ln \frac{eR}{r} \tag{7}$$

and

$$R = 0.122 (K_I/\sigma_Y)^2 \tag{8}$$

was obtained.

The node closest to the crack tip has been excluded. The difficulties in obtaining a consistent result near the tip may be explained by the relative coarseness of the mesh at this point. The amplitude 3.11 should be compared to the value 2.76 for the perfectly plastic material[11] which was determined for the case of small scale yielding through an examination of the velocities in the Prandtl slip line field.

At a FEM investigation continued from the steady state situation the load is (a) decreased to 0.6 of full load, (b) removed completely and then fully restored. (a) and (b) are followed by crack growth simulated by a node relaxation technique. For a reference case, crack growth is also simulated by node relaxation immediately following the moving mesh solution without any interrupting changes in external load.

Unloading - reloading

During unloading contact forces must be introduced to prohibit overlapping. The extension of the contact region is rather small for loads larger than about $0.4K_{Io}$. At the end of the analysis when the remote load is completely removed,

Immediately as the load is decreased from the steady state situation the complete plate becomes elastic, and it is not until below $0.4K_{Io}$ that the material behavior becomes plastic at one integration point. The secondary plastic zone present at steady state remains elastic throughout the unloading process.

In the following analysis the initial load is restored. During this part, as in the first phase of the analysis, the crack is assumed not to grow. The reloading induces large changes in plastic strain distribution. Evidently the process is not reversible. A study of Figure 9 reveals large deviations in the crack surface displacement during reloading compared with unloading at corresponding loads. Excessive blunting of the crack tip is observed. This is manifested by a displacement $0.30K_I^2/E\sigma_Y$ of the node closest to the crack tip, which can be compared with the result[13] $0.33K_I^2/E\sigma_Y$ for a static virgin crack.

Continued crack growth at unchanged load. $K_I = K_{Io}$

Continued crack growth is studied by means of a nodal relaxation technique. In order to eliminate errors due to the change of FEM technique, node relaxation is first used to simulate crack growth immediately following the moving mesh analysis, hence leaving out the removal and restorage of remote load.

The crack surface displacement is slightly larger when the node relaxation technique is used than with the moving mesh technique (see Figure 10). The best approximation to the least squares method is given by:

$$v_a = 2.85 \frac{\sigma_Y}{E} r \ln \frac{eR}{r} \qquad (9)$$

with

$$R = 0.166 (K_I/\sigma_Y)^2 \qquad (10)$$

The solution (9) with

$$R = 0.166\ (K_I^e/\sigma_Y)^2 \qquad (11)$$

where K_I^e is an equivalent stress intensity factor, is below replacing the radial dependence r^s (cf. eqn. (3)) in the approximation for the displacements. Thus $K_I^e = K_I$ at continued steady state crack growth although K_I^e can also be calculated at each step of the continued crack growth, e.g. when 2, 4, 6 and 10 nodes were relaxed. Figure 11 shows that K_I^e is rather constant (only slightly lower than K_I when only two nodes were relaxed).

Continued crack growth at $K_I = 0.6K_{Io}$.

A crack that experiences steady state crack growth, then instantaneously decreased load to $0.6K_{Io}$ followed by continued crack growth by relaxation of nodes, is studied. As the first two nodes are relaxed the displacement for these nodes decreases, i.e. the crack surfaces overlap. This is of course an unrealistic situation. The implications are not fully understood, and we are submitted to speculation on why continued crack growth is observed in experiments. On possibility might be that microcracks or voids that later coalesce with the main crack, region ahead of the crack tip. Assuming that (9) and (11) define the crack surface displacements in the crack tip neighbourhood also shortly after a load transient, K_I^e can easily be obtained. Figure 11 shows that K_I^e changes significantly during continued crack growth, increasing from a rather small value to a value very close to the value expected at steady state crack growth at $0.077(K_{Io}/\sigma_Y)^2$.

When ten nodes are relaxed the height of the plastic zone is $0.046(K_{Io}/\sigma_Y)^2$ which equals $0.13(K_I/\sigma_Y)^2$. This should be compared with the height $0.16(K_{Io}/\sigma_Y)^2$ at steady state.

Continued crack growth at $K_I = K_{Io}$ after an intermediate unloading-reloading process

It is of interest to compare this last case with the reference case for which the moving mesh technique was instantaneously replaced with the node relaxation technique for steady state solutions, since unloading-reloading has been recommended as a method for breaking conductive bridges at the crack surface.

The excessive blunting observed at the reloading process results after some amount of crack growth as an indentation of the width $0.018(K_{Io}/\sigma_Y)^2$ and the depth about $0.32\ K_{Io}^2/E\sigma_Y$ at four relaxed nodes, and the width $0.022(K_{Io}/\sigma_Y)^2$ and the depth about $0.29K_{Io}^2/E\sigma_Y$ at ten relaxed nodes (see Figure 10). The crack surface displacements are larger than at steady state on the trailing side of the indentation and the difference is almost constant for $x > -0.15(K_{Io}/\sigma_Y)^2$. Thus the difference is $0.09K_{Io}^2/E\sigma_Y$ at $x = -0.04(K_{Io}/\sigma_Y)^2$, and $0.07K_{Io}^2/E\sigma_Y$ at $x = -0.10(K_{Io}/\sigma_Y)^2$

before continued crack growth, and $0.10K_{Io}^2/E\sigma$ at $x=-0.04(K_{Io}/\sigma_Y)^2$, and $0.08K_{Io}^2/E\sigma_Y$ at $x=-0.10(K_{Io}/\sigma_Y)^2$ after ten relaxed nodes. Even though the strain field is considerably redistributed, K_I^e is comparatively constant at continued crack growth, only slightly lower when only two nodes are relaxed.

SIMULATION OF CRACK GROWTH IN CERT SPECIMENS

Frequently average crack growth rates from CERT tests are reported, and it may be asked whether these values are of any interest for prediction purposes. It is easily recognized that the situation in a CERT specimen is well beyond small-scale yielding and thus cannot be directly compared to results from testing of CT specimens. In order to explore the possibilities to use crack growth data from CERT testing for quantitative purposes, a finite element simulation was performed. Since in a CERT test no measurements of the crack growth are made, the assumption was made that growth initiation occured after 60 hours, and then the growth was constant and equal to $2.6\ 10^{-9}$ m/s corresponding to a total growth rate of 1.0 mm during a test. This is a value typical of tests when IGSCC occurs in clean BWR environment with 200 ppb O_2. The simulation was performed by ABAQUS, and the axisymmetric finite element model is shown in Figure 1. The mesh contains 302 elements and 1086 nodes. The growth is simulated by gradual nodal release as described previously. Since a comparison with the small-scale yielding analyses was desired, the calculation was performed under small deformation assumptions, unlike the calculations on the uncracked CERT specimen reported above. In Figure 12 the crack surface displacements for some different crack lengths are shown. A tendency for fluctations as compared with a smooth curve is observed, the midside nodes of the elements giving relatively smaller displacements than the corner nodes. The same tendency, although less marked, was observed in the small scale yielding analysis and is believed to be due to the relaxation procedure. In this the nodal forces at both midside and corner nodes are relaxed proportionally, whereas a more rapid release of the corner nodal force would be more appropriate.

As a basis for comparison with the small scale yielding situation the crack surface displacement is used. Thus a curve of the form (9) is fitted to the displacements from the FEM calculations. Since considerable hardening occurs, the comparison could not be performed on basis of the virgin yield stress. The tangent modulus, however, is low so the variation of the current flow stress along the crack surface is small. Thus a fitting based on eqn. (9) with an updated value of the yield stress should be reasonable. Both σ_Y and K_I^e were varied in the fitting process using a non-linear least squares procedure from the NAG library[14]. The

fitted curves are shown in Figure 12.

In Figure 13 the effective value K_I^e as determined from the fitting is shown as function of the crack length. The values increase rapidly with crack length and reach very high values. Thus it is unlikely that the assumption of constant crack growth rate is correct. Furthermore it is observed that, except for very short lengths, the K_I^e values are unrealistically high. Thus a comparison with small scale yielding results appears meaningless. The main conclusion to be drawn from this qualitative analysis is that the conditions at a tip of a growing crack in a CERT test are very far from what can reasonably be achieved under practical situations, and that the growth rates observed in CERT tests are of little or no value for prediction purposes.

DISCUSSION

One prominent feature of the numerical analysis of the uncracked CERT specimen is the very high stress and the high degree of triaxiality at the bottom of the notch. Such high values can never be achieved in an unnotched specimen. On the other hand, the calculated strain at the estimated time of crack initiation (7 percent) is roughly comparable to results for unnotched specimens[15]. This suggests that strain is more important than stress for initiation of stress corrosion cracks, which is consistent with the current theoretical models[16].

The analysis of crack propagation in CERT tests showed that there is no basis for comparison with CT testing. The effective values of the stress intensity factors K_I^e are far beyond what can reasonably be encountered in a practical situation. Furthermore as can be seen from Figure 12 the crack tip opening angles are quite large (of the order of 10 degrees) which may counteract the formation of crevice conditions. The situation is thus so different in CERT tests, as compared to CT tests, that even the use of the CERT test for ranking purposes could be considered as open to discussion. However, practical experience from many years of testing and field behavior seems to show that CERT is useful for ranking purposes.

A severe decrease in stress intensity was observed at the analysis of a growing crack subjected to a sudden decrease in remote load. The equivalent stress intensity factor K_I^e shows a gradual recovery during continued crack growth and at a point $0.08(K_{Io}/\sigma_Y)^2$, K_I^e has reached about the same level as for steady state at the same remote load.

These changes in K_I^e are likely to produce a similar behavior in the crack growth rates, which is consistent with the experimental observations. The initiation immediately after the decrease in remote load cannot, however, be

explained by the idealized model chosen for analysis since compressive stress is present ahead of the crack tip. After a forced crack growth of about $0.01(K_{Io}/\sigma_Y)^2$ the compressive stress is replaced with a tensile stress.

After an unloading-reloading cycle the crack tip becomes considerably blunted, almost as much as when loading a static virgin crack. This might support the suggestion made earlier in this paper that either mechanical or electrical connections are developed between the crack surfaces during steady state crack growth. The explanation should then be that these connections are broken as the crack surface displacement is much larger after the unloading-reloading cycle.

CONCLUSIONS

* The stress state in the notched CERT test is quite different from that of the unnotched specimen. However, crack initiation seems to occur at roughly the same strain levels in both cases.
* The crack propagation process in the CERT test cannot be related to CT tests, and average growth rates should not be used for prediction purposes.
* At a partial unloading in a CT test the analysis predicts a considerably lower growth rate than that corresponding to the new steady state level. After a recovery period of the order of the plastic zone size the steady state level is reached again.
* A significant separation of the crack surfaces results after the load is removed and applied again. The crack tip is severely blunted. Even though there are significant changes in strain distribution the equivalent K_I^e appears to be rather unaffected.
* FEM calculations seem to be a useful tool for analysis of stress corrosion processes.

ACKNOWLEDGEMENTS

The experimental work was sponsored by the Electric Power Research Institute and the Swedish Nuclear Power Inspectorate. The latter organization also sponsored the numerical calculation work. The authors wish to express their gratitude for this support.

REFERENCES

1. G. M. Ugiansky, J. H. Payer, editors, ASTM STP 665, Philadephia, PA, 1979.
2. P. L. Andresen, General Electric Report 81CRD042, March 1981.
3. L. G. Ljungberg, D. Cubicciotti, M. Trolle, CORROSION/87, Paper No. 108, NACE, Houston, Texas, 1987.

4. W. E. Ruther, W. K. Soppet, T. F. Kassner, CORROSION/85, Paper No. 102, NACE, Houston, Texas, 1985.
5. M. E. Indig, G. M. Gordon, R. B. Davis, Proc. of Materials in Nuclear Power Systems, NACE, Houston, Texas, p. 506, 1983.
6. N. Ohnaka et al, Boshoku Gijutsu, Vol. 32, No. 4, p. 214 (1983).
7. L. G. Ljungberg et al, Proc. of 2nd Int. Symp. on Environmental Degradation of Materials in Nuclear Power Systems, NACE, Houston, Texas, p. 435 (1985).
8. ABAQUS, User's Manual, version 4.5, Hibbitt, Karlsson and Sorensen Inc., Providence, RI02906, 1985.
9. G.C. Nayak, O.C. Zienkewicz, Int. Journal for numerical Methods in Engineering, Vol. 5, p. 113, 1972.
10. P. Ståhle, Report from the Division of Solid Mechanics, TFHF-3020, Lund Institute of Technology, Lund, Sweden, 1985.
11. W. J. Drugan, J. R. Rice, T. L. Sham, J. of the Mech. and Phys. of Solids, Vol. 30, p. 447 (1982).
12. P. Ponte Castaneda, J. of the Mech and Phys. of Solids, Vol. 35, p. 227 (1986).
13. J. R. Rice, E. P. Sorensen, J. of the Mech. and Phys. of Solids, Vol. 35, p. 163 (1978).
14. NAG, Mark 9, Vol. 3, Numerical Algorithms Group Ltd, Oxford,UK, 1982.
15. P. L. Andresen, Corrosion, Vol. 38, p. 53 (1982).
16. F. P. Ford and N. Silberman, Corrosion, Vol. 36, p. 558 (1980).

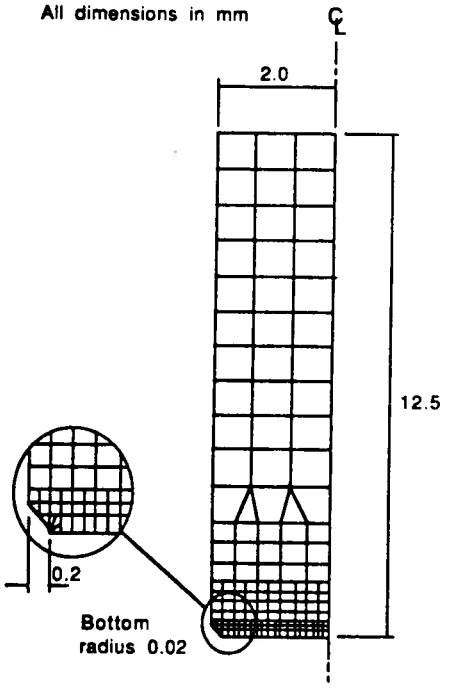

FIGURE 1 - Upper half of CERT specimen used in ASEA-ATOM tests.

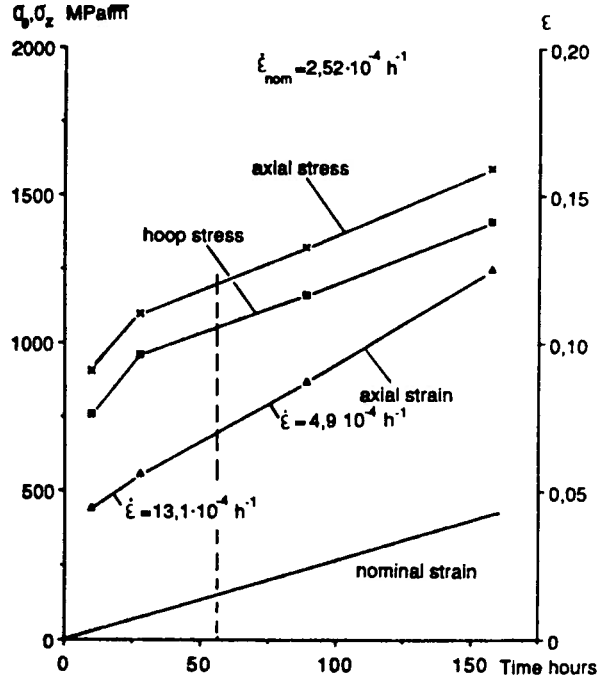

FIGURE 2 - Maximal axial stress and strain in the notch as a function of time.

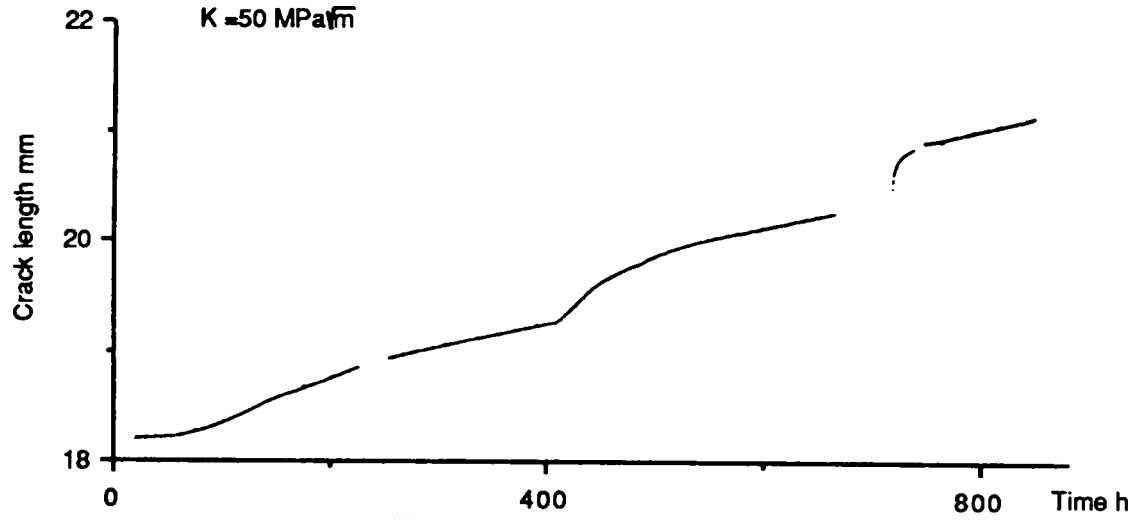

FIGURE 3 - Crack propagation in COL specimen tested in normal BWR water with H_2SO_4. The H_2SO_4 concentration initially was 25 ppb. At 400 hours it was increased to 100 ppb. At 700 hours the specimen was unloaded and reloaded once.

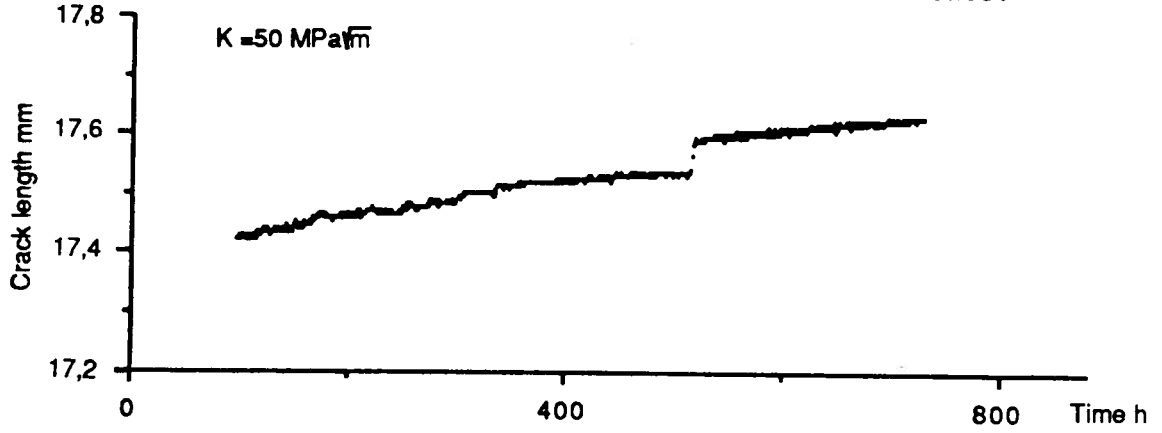

FIGURE 4 - Crack propagation in COL specimen tested in normal BWR water with 100 ppb H_2SO_4 at 288^0C. K_I = 25 MPa $m^{1/2}$. The specimen was unloaded for a short time at 450 hours.

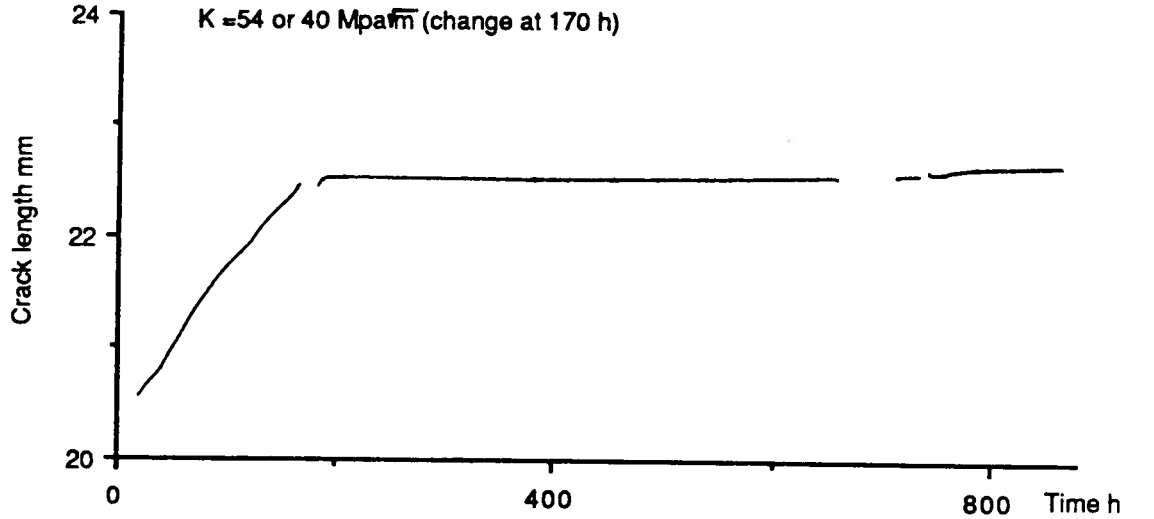

FIGURE 5 - Crack propagation in COL specimen tested in normal BWR water with 25 ppb H_2SO_4 at 288^0. The decrease in load is by 170 hours. By 500 hours to 700 hours the crack slowly starts to grow again.

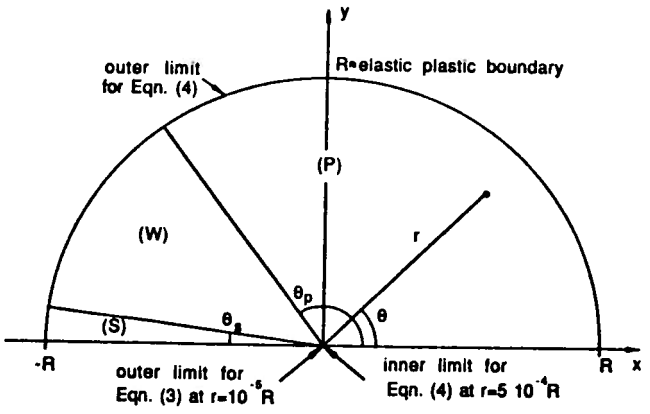

FIGURE 6 - The regions of application for the approximations Eqns.(3) and (4). Polar coordinates r, θ are attached to the tip.

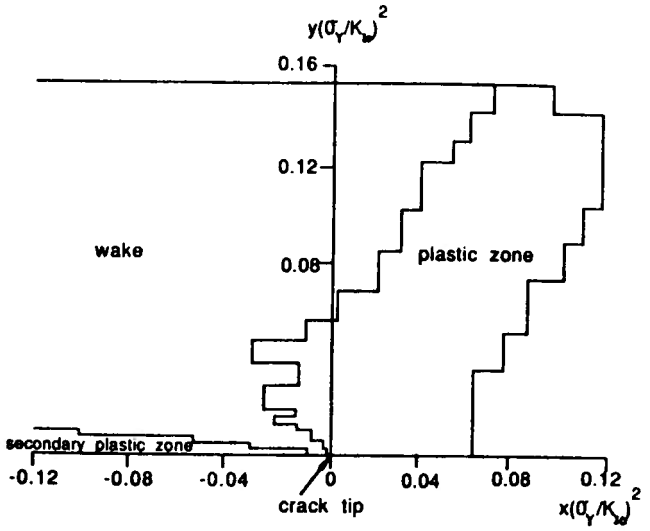

FIGURE 7 - Shape of the plastic zone at steady state.

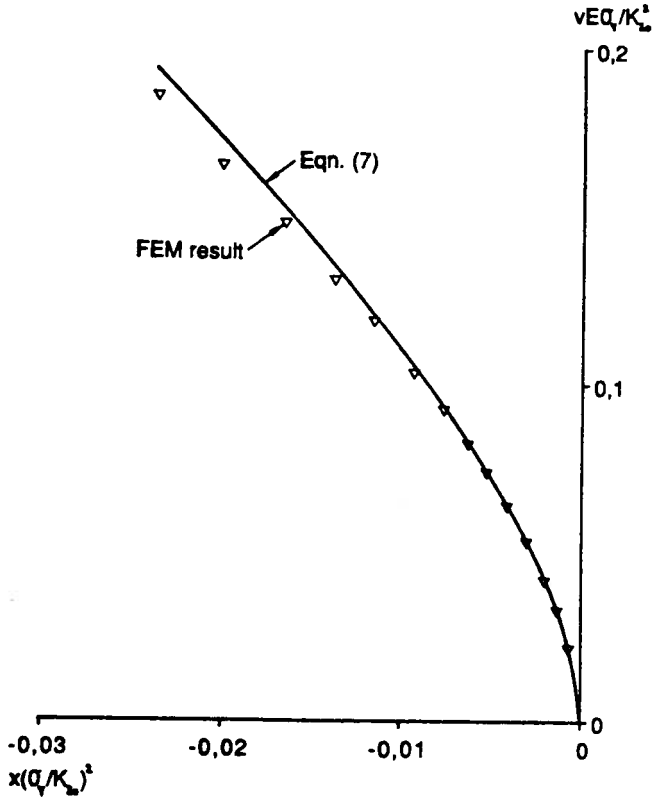

FIGURE 8 - Crack surface displacements at steady state. The approximation Eqn. (7) is included.

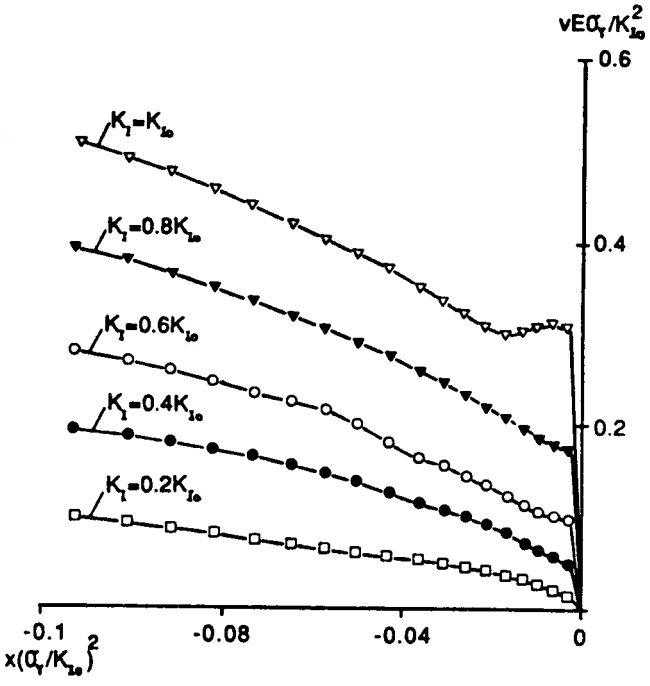

FIGURE 9 - Crack surface displacements during reloading.

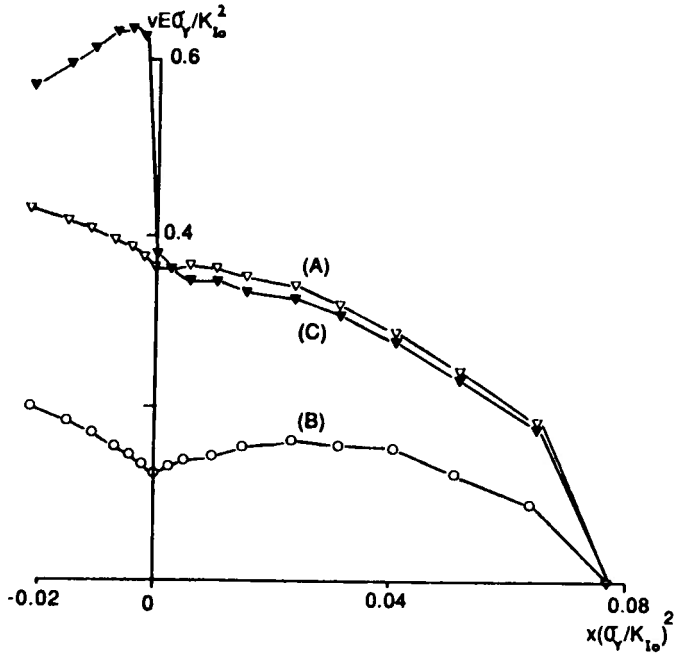

FIGURE 10 - Crack surface displacements during continued crack growth (A) without any changes in remote load, (B) after a decreased load to $0.6K_{Io}$ and (C) after an unloading-reloading cycle.

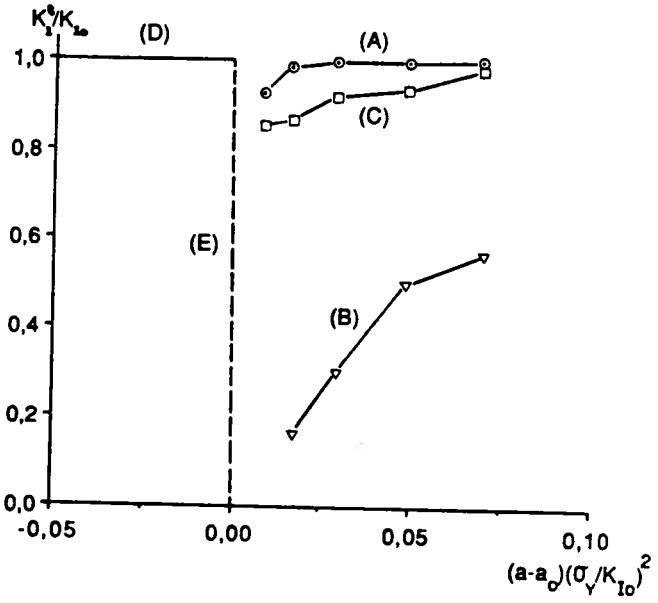

FIGURE 11 - Equivalent stress intensity factors for the cases in Figure 10. (D) represents the steady state situation before the load transient and (E) representing the unloading-reloading cycle.

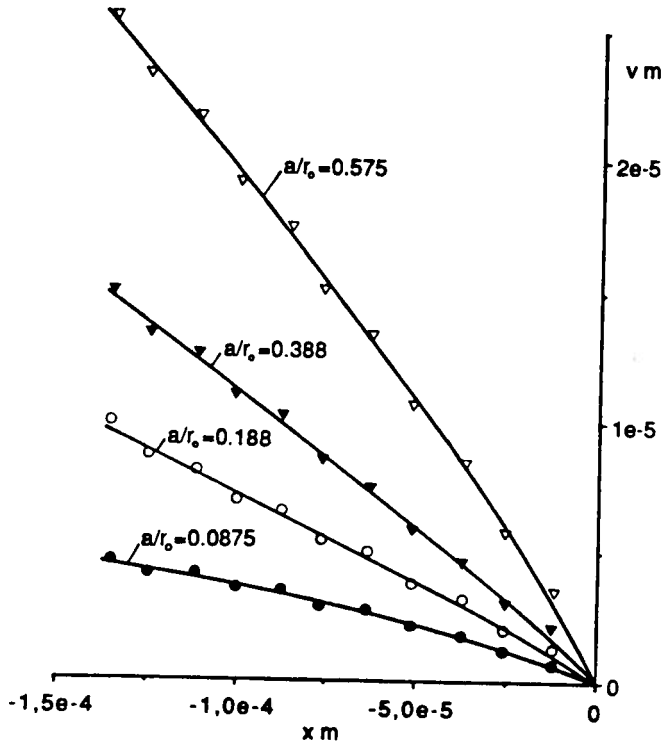

FIGURE 12 - Crack surface displacements for some crack lengths in simulation of CERT test.

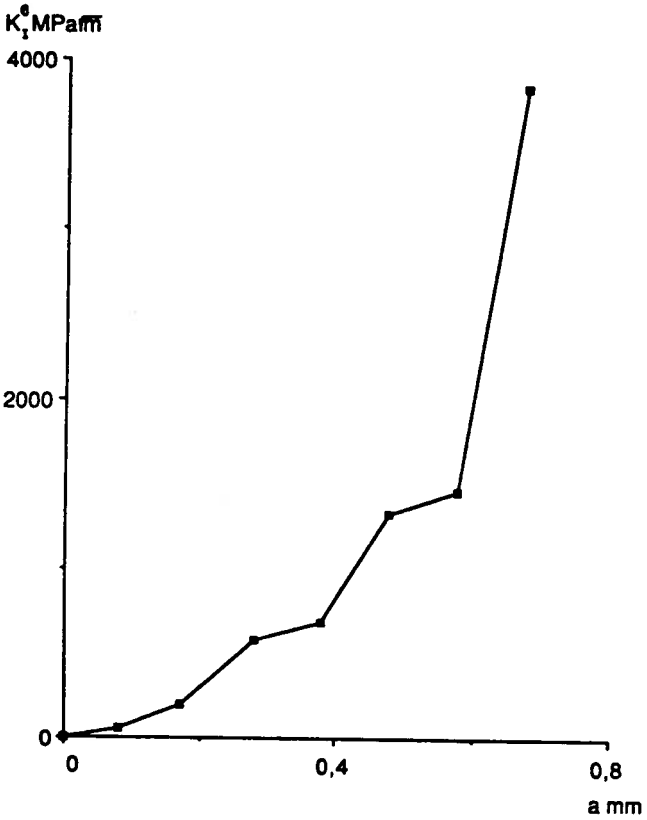

FIGURE 13 - The apparent K_I^e value as a function of crack length for the CERT test.